Journal of Catalysis 282 (2011) 13–24

Contents lists available at ScienceDirect

Journal of Catalysis

journal homepage: www.elsevier.com/locate/jcat

Kinetic studies of the stability of Pt for NO oxidation: Effect of sulfur and long-term aging

Jorge H. Pazmiño [a], Jeffrey T. Miller [b], Shadab S. Mulla [a], W. Nicholas Delgass [a], Fabio H. Ribeiro [a,*]

[a] School of Chemical Engineering, Purdue University, 480 Stadium Mall Drive, West Lafayette, IN 47907-2100, USA
[b] Chemical Technology Division, Argonne National Laboratory, 9700 S. Cass Avenue, Argonne, IL 60439, USA

ARTICLE INFO

Article history:
Received 10 February 2011
Revised 2 May 2011
Accepted 4 May 2011
Available online 12 June 2011

Keywords:
NO oxidation
Sulfur
EXAFS
Pt oxidation
Deactivation
Stability

ABSTRACT

The stability of Pt catalysts for NO oxidation was analyzed by observing the effect of pre-adsorbed sulfur on the reaction kinetics using a series of Pt/SBA-15 catalysts with varying Pt particle sizes (*ca* 2–9 nm). Our results indicate that sulfur addition did not influence catalyst deactivation of any of the Pt catalysts, resulting in unchanged turnover rates (TOR) and reaction kinetics. The presence of sulfur on Pt was confirmed by X-ray absorption fine structure spectroscopy (EXAFS) under reducing environments. However, exposure of the catalyst to NO oxidation conditions displaced sulfur from the first coordination shell of Pt, yielding Pt–O bonds instead. Re-reduction fully recovered the Pt–S backscattering, implying that sulfur remained near the Pt under oxidizing conditions. X-ray photoelectron spectroscopy (XPS) and chemisorption measurements confirmed the presence of sulfur near platinum. The invariance of the NO oxidation reaction to sulfur poisoning is explained by sulfur displacement to interfacial sites and/or sulfur binding on kinetically irrelevant sites. Formation of Pt oxides remains as the main source of catalyst deactivation as observed by kinetic and X-ray absorption spectroscopy (XAS) measurements.

1. Introduction

NO oxidation over supported Pt catalysts plays a key role in developing NO_x abatement technologies for lean-burn engines, such as the NO_x storage reduction (NSR) catalysts [1]. Given the increasing market prices for Pt and other noble metals, broad commercialization of NSR catalysts still requires further improvements, especially in terms of durability and resistance to poisons. The presence of sulfur-containing compounds in fuel and lubricants has been reported to favor the formation of thermally stable sulfate species on NO_x storage sites, detrimentally affecting catalyst performance [2–4]. Such an outcome has been reported to occur to similar extents when SO_2, H_2S, or COS were introduced, with rich conditions causing greater catalyst deactivation as compared with lean periods [5–8]. Regeneration of sulfur-poisoned catalysts usually requires high-temperature processes that lead to thermal aging of the catalyst by Pt sintering and/or reaction of the storage component with the support [9–11]. Sulfur has also been reported to affect the metal functionality for NO oxidation [12–17]. While SO_2 has been shown to severely decrease the activity on rhodium-based catalysts [18,19], discrepancies still remain regarding the effect of sulfur on Pt catalysts. For example, Engström et al. [3] reported an inhibition effect of SO_2 on the NO oxidation activity on a $Pt/Rh/BaO/Al_2O_3$ possibly caused by site blocking. Under similar experimental conditions, Amberntsson et al. [6,12] observed an increase in oxidation activity with the addition of SO_2 on $Pt/BaO/Al_2O_3$ and $Pt/Rh/BaO/Al_2O_3$ and concluded that the enhancement in NO_2 formation was caused by an increased resistivity to Pt oxidation. However, in later studies [13,16] done by the same group, the inclusion of SO_2 in the NO_x mixture showed a detrimental effect in the short time range and a slow recovery of activity in the long term due to S-promoted platinum sintering. These contradictory observations may be related to changes in platinum–sulfur interactions with varying conditions and/or to contributions from the storage component in the vicinity of Pt. In their kinetic study, Ji et al. [14] reported a total suppression of NO oxidation activity upon the addition of SO_2 in the feed. When SO_2 was introduced prior to reaction, the activity of Pt/SiO_2 was mostly restored, while only a partial regeneration was observed on Pt/CeO_2. Their results pointed out the preferential oxidation of SO_2 over NO and the effect of support in catalyst regeneration. However, their kinetic analysis was biased by the exclusion of the product NO_2 in the feed stream to account for product inhibition. Evidently, the effect of sulfur on the catalytic role of Pt for the NO oxidation reaction still requires a systematic kinetic evaluation without the complexities derived from supports with high affinity for sulfur, such as Al_2O_3 [20–23] or BaO/Al_2O_3 [7,9,24].

Sulfur adsorption on platinum has been widely studied on supported and single-crystal catalysts [25]. Wang et al. [26] showed

* Corresponding author.
E-mail address: fabio@purdue.edu (F.H. Ribeiro).

0021-9517/$ - see front matter © 2011 Elsevier Inc. All rights reserved.
doi:10.1016/j.jcat.2011.05.007

that bulk sulfides are readily formed on SiO_2-supported Pt, Pd, and Rh catalysts upon heating in 10%H_2S/N_2, reaching complete surface sulfidation at 300 °C. Also, they found that sulfides are partially transformed to $PtSO_4$ and PtO after calcinations in air at 300 °C and that complete removal of sulfur was achieved at 500 °C. Other studies on Pt (1 0 0) and (1 1 1) crystals [27,28] have also observed sulfur adsorption with saturation coverage ranging from 0.4 to 1. Their results suggest that more sulfur was adsorbed at lower temperatures, reaching sulfur coverage (θ_s) of 0.92, but heating above 300 °C resulted in the desorption of weakly bonded S resulting in a θ_s of 0.38–0.5. Given the high affinity of Pt to form stable compounds with sulfur, saturation coverage can be achieved with P_{H2S}/P_{H2} in the order of 10^{-8} between 200 and 300 °C [25]. Catalyst supports can form stable sulfates either by direct reaction at high temperatures (>700 °C) or as a result of oxidation of sulfur on the Pt surface and spillover SO_x species. Therefore, depending on the capacity of the support to store sulfur, platinum will be more or less susceptible to be poisoned.

The chemical state of adsorbed sulfur has been reported to be dynamic, changing with reaction environments. For example, EXAFS measurements taken by Gracia et al. [22] on a highly dispersed Pt/SiO_2 catalyst for CO oxidation suggested that adsorbed sulfur existed in two configurations depending on the reaction atmosphere: (i) directly bonded to Pt under reducing conditions and (ii) through an oxygen atom as Pt–OSO_x when oxidized. Sulfur can also modify the structure and electronic properties of platinum and interact with the support as well. Many studies [29–32] have reported on S-induced surface reconstruction and particle agglomeration due to lowering of the surface free energy for the sulfided Pt. Similarly, sulfur modifies the co-adsorption of other molecules such as, H_2, O_2, and CO. These molecules are of particular interest for many reactions as they participate as reactants and/or they are used to quantify the surface metal atoms by chemisorption techniques. In that regard, Apesteguia et al. [33] reported that in the case of sulfided Pt/Al_2O_3 catalysts, the Pt surface area calculated by H_2 chemisorption was significantly lower than the values from O_2 and CO chemisorption.

Considering that NSR catalysts are designed to perform over long periods of time, it is also relevant to gain a better understanding of sulfur regenerability and catalyst stability. Partial sulfur removal has been reported on Pt/Al_2O_3 catalysts upon reduction treatments with H_2 at temperatures above 350 °C, while oxidation prior to low-temperature reduction was seen to completely remove the sulfur from the metal [34,35]. The mechanism of regeneration was proposed to occur via the formation of sulfates on the Al_2O_3 support [34], a material that is known to interact with sulfur. Apart from any sulfur effects on catalyst performance, platinum-based formulations have been shown to deactivate over time under NO oxidation conditions. Previous studies on non-sulfided catalysts [36–38] have attributed the decrease in catalytic activity for NO oxidation to the oxidation of Pt particles (as seen by XPS) promoted by the presence of NO_2. In fact, Segner et al. [39] and Parker and Koel [40] have shown that NO_2 is a very effective source of surface oxygen because of its high sticking coefficient. As a result, NO_2 is known to kinetically inhibit the reaction as it competes for adsorption sites for O_2 [41]. The inhibition effect, however, cannot explain the persistent deactivation with time observed in studies where the product NO_2 was included in the feed [37]. Such instability has also been reported to occur over long time periods, complicating the collection of reproducible kinetic measurements [16,42]. Other researchers [43] have suggested that platinum remains metallic regardless of the cluster size over a large range of oxygen virtual pressures and suggest that deactivation could be related to impurities in the NO_2-containing gas mixture, possibly in the form of bromine or chlorine species [44].

To provide a better insight into the effect of sulfur on NO oxidation and the nature of catalyst instability, we make use of kinetic analysis and spectroscopic techniques (XPS, XAS) to investigate the chemical state of Pt under NO oxidation conditions. Our approach consists of (i) using Pt/SBA-15 catalysts to study the effect of sulfur and the regenerability of the Pt under operating conditions and (ii) assessing the nature of deactivation and its effects on kinetic parameters over long times by using a non-sulfided Pt/Al_2O_3 monolith catalyst.

2. Experimental methods

2.1. Catalysts

The 1%Pt/SBA-15 catalysts with average particle size of 3.8 and 9.0 nm were provided by Professor R.M. Rioux. The samples were prepared by a solution-based alcohol reduction method, which allows sufficient control over the metal particle size to tune it to the mesoporous SBA-15 silica support pore diameter [45]. Synthesis and incorporation of Pt nanoparticles in the mesoporous silicate support were done using low-power sonication. The Pt/SBA-15 with an average Pt particle size of 2.3 nm was prepared by incipient wetness impregnation as follows: after mixing 1 g of SBA-15 with 50 mL of H_2O, 1 mL of NH_4OH (pH > 10) was added and mixed for 30 min. Once a homogeneous SBA-15 slurry was formed, a solution containing 0.02 g of $Pt(NH_3)_4(NO_3)_2$ dissolved in 25 mL of H_2O and 0.5 mL of NH_4OH was added, and the mixture was stirred for 30 min at room temperature. The resulting solid was filtered and rinsed twice with 50 mL of H_2O and then dried at 125 °C overnight. The sample was later calcined in flowing air at 200 °C for 2 h and reduced at 250 °C for 1 h. Before exposing the catalyst to the room conditions, He was flown at 250 °C to desorb H_2, and the sample was cooled to room temperature in He. To simplify catalyst notation, the particle size of the S-free catalysts was used to differentiate each set of Pt/SBA-15 and its corresponding sulfided samples. For example, Pt/SBA-2.3-S refers to 2.4%Pt/SBA-15 with mean Pt particle size of 2.3 nm, which was subjected to the H_2S/H_2 treatment described in Section 2.5.

The Pt/Al_2O_3 catalyst in the monolithic form was supplied by EmeraChem. The monolith was dipped into an aqueous slurry, which contained the appropriate amount of γ-Al_2O_3 based on a known liquid uptake of the bare monolith. The monolith was then drained, dried, and calcined in flowing air at 500 °C for 1 h. Deposition of Pt was done by dipping the treated monolith into a Pt-containing aqueous solution in such a way that the final Pt loading was approximately 1.8×10^{-3} g cm^{-3} of monolith. An amine-based solution was used as the Pt precursor. The resulting monolith had a Pt loading of ca. 0.3 wt.% and a cell density of 31 channels cm^{-2}. The fraction of Pt surface metal to the total Pt atoms was measured using the CO titration technique described in the next section.

2.2. Metal dispersion measurements by CO titration, H_2 chemisorption, and H_2 titration

CO titration experiments were conducted in the NO oxidation reactor, which is described in Section 2.3. The catalysts were subjected to an oxygen exposure at room temperature with 30% O_2/N_2 (1 L min^{-1}) for 1 h. According to Benson and Boudart [46], this room-temperature oxygen exposure leads to a monolayer of adsorbed oxygen on Pt with an O/Pt_S ratio of unity. After this pre-treatment with oxygen, the flow was switched to Ar (750 mL min^{-1}) in order to purge out any residual gases from the pre-treatment, and the reactor temperature was set to 150 °C. At this titration temperature, the flow was changed to 3% CO/Ar (750 mL min^{-1}), and the exit gases were analyzed in an FT-IR gas

analyzer (Thermo Electron Corporation, Nicolet Antaris IGS) for CO_2. The CO_2 trace was followed until it decreased to below the detection limit (typically about 10 min). The resulting CO_2 trace was integrated and, assuming a reaction stoichiometry $CO + O–Pt_S \rightarrow CO_2 + Pt_S$, the total amount of oxygen on the Pt was calculated. At 150 °C, CO can titrate the oxygen monolayer completely from Pt, and hence, the CO_2 amount formed (or the atomic oxygen removed) will be the same as the number of exposed surface Pt atoms [37]. It is thus possible to calculate the number of surface Pt atoms from the CO titration at 150 °C and consequently the Pt dispersion (ratio of surface Pt to total Pt) while the catalysts are still in the reactor. The Pt average particle size was then calculated as (d in nm $\approx$ 1.1/dispersion).

Following the standard methods for H_2 chemisorption and H_2–O_2 titration, the Pt surface area for clean and sulfided catalysts was determined [46]. The measurements were taken on a Micromeritics ASAP 2020 instrument. The reduction temperature was 250 °C for all catalysts, and the maximum temperature for evacuation was set at 200 °C as a precaution in case sulfur were to desorb from the samples and contaminate the analysis manifold. Hydrogen chemisorption was done at 35 °C. Upon completion of the H_2 chemisorption experiment, the catalyst was purged in He, heated to 100 °C, and oxidized in UHP O_2 for 30 min at 100 °C. Titration with hydrogen was subsequently performed at 100 °C.

2.3. Reactor setup

The reactor system was designed to operate with two types of reactors depending on the form of the catalyst. For the monolith catalyst, a bench-top, plug-flow stainless steel reactor (2.6 cm in OD) was used for measuring the conversion of NO. The monolith was wrapped with high-temperature Zetex insulation to minimize the gas flow bypassing the catalyst. A 6–8-cm bed containing clean glass beads was placed upstream in the reactor to ensure uniformity of the mixture inlet gas. The reactor was placed inside a temperature-controlled furnace, and a pre-heater was used before the reactor to avoid temperature gradients along the monolith. The temperature was monitored upstream and downstream of the monolith with two K-type thermocouples, each at a distance of 6 mm with respect to the edge of the sample. A reactor bypass line located after the pre-heater was used to measure the inlet concentrations of NO and NO_2 after each catalyst evaluation. The gas-phase bypass concentrations were used as the inlet concentrations for all the rate calculations in order to account for the reaction over the catalyst.

The reactor design for powder samples consisted of a bench-top, plug-flow 1.3-cm-diameter vertical Pyrex reactor with a 190–233-μm glass frit fitted at the midpoint of the reactor to support the powdered catalysts. Since the particle size of some of the powder catalysts was smaller than the openings of the glass frit, a thin (about 2 mm) plug of clean quartz wool was placed over the frit in order to support the catalyst powder. The two ends of the 1.3-cm-diameter glass reactor were joined to a 7.6-cm-long, 2.6-cm-OD-diameter, thick-walled glass tubing. The reactor was cleaned prior to loading the catalyst with a phosphate-free cleaning solution, followed by pouring in fresh *aqua regia* followed by rinsing with DI water and drying. A 4–5-mm-deep bed of glass beads was supported on a metallic mesh located at 1 cm above the catalyst. Another layer of quartz wool was added on top of the catalyst and slightly pressed against it to ensure uniformity of the bed. In order to maintain isothermal conditions across the catalyst bed, a 19-cm-long aluminum sheath was placed around the 1.3-cm-diameter portion of the glass reactor. In addition, the glass was wrapped with a 5-cm-long aluminum foil centered in the portion of the reactor where the catalyst bed was located. Two K-type thermocouples were placed at ~2 mm above the catalyst bed and right below the quartz frit. Mass flow controllers were used to control all the gas flows, and their concentrations were varied by adjusting their respective flow rates. A pressure gauge with an analog output was used to monitor the feed pressure to the reactor.

2.4. Reaction kinetic measurements

The monolith catalyst was pre-treated at 250 °C with 10% O_2 in N_2 for 1 h to oxidize any carbonaceous impurities, followed by reduction with 0.5–1% H_2 in N_2 for 1.5 h with a constant total flow rate of 6.6 L min^{-1}. For the powder samples, the pre-treatment in 10% O_2/N_2 and the reduction in 1%H_2/N_2 were done at 340–350 °C, at a total flow rate of 3.5 L min^{-1}. The reactor was operated in a differential regime by keeping the NO conversions below 10% and by including NO_2 in the feed to minimize the contribution of the NO_2 formed to the total NO_2 concentration. The NO and NO_2 concentrations in the outlet gas were detected with a FT-IR gas analyzer (Thermo Electron Corporation, Nicolet Antaris IGS). Factory-supplied calibrations were used for the analysis of the spectra collected at a resolution of 0.5 cm^{-1}. The kinetic measurements at different gas composition or temperature conditions were taken after the catalyst was on stream for at least 1 h, once the sample has been stabilized. Stabilization treatments consisted of exposing the catalysts to reaction conditions for at least 16–18 h. The repeatability of the measurements was checked by periodically returning to a base case condition (300 ppm NO, 170 ppm NO_2, 10%O_2, balance N_2, 3.4 L min^{-1}, 1 atm) at a chosen temperature (generally 300 °C). Acceptance of data as stable required repeatability of the base case condition over the entire time period of the experiment. We were not able to use the Madon–Boudart [47] test to verify experimentally that no heat and mass transport limitations were present, because of the sensitivity of rates with dispersion and deactivation. Instead, the criteria proposed by Dekker et al. [48] were used for both the monolith and powder samples. Detailed calculations reported in the Supplemental information confirmed negligible transport effects. All parameters were obtained from direct measurements, correlations [49], or data from handbooks [50].

The estimate of the apparent activation energy at low and high reaction temperatures was determined from data collected between 150–200 °C and 250–320 °C, respectively. The temperature was varied in a random fashion while maintaining the standard feed composition at 300 ppm NO, 170 ppm NO_2, 10% O_2, and balance N_2 with a total flow rate of 6.6 L min^{-1} for the monolith and 3.4 L min^{-1} for the powder samples. The reaction orders were obtained by performing one-component-at-a-time variation experiments over the ranges 150–420 ppm for NO, 5–30% for O_2, and 120–420 ppm for NO_2, at a constant baseline temperature of 160 °C for Pt/Al_2O_3 monolith or 300 °C for Pt-SBA-15 catalysts. Least-squares analysis of the Arrhenius plot and the linear form of the power law expression were used to estimate the apparent activation energies, orders of reaction, and their confidence limits.

2.5. Ex situ sulfur pre-treatment

The Pt/SBA-15 powder catalysts were treated in an independent bench-top, plug-flow, 1.3-cm-diameter vertical Pyrex reactor assigned only for sulfur treatments. The choice of catalyst for S poisoning was based on earlier findings that concluded that SiO_2 supports are less susceptible to the formation of surface sulfates compared to Al_2O_3 or TiO_2 [20,22]. Therefore, sulfur will interact mostly with Pt instead of being stored in the support. With the aid of a separate temperature-controlled furnace, the fresh catalysts were pre-treated with H_2S under either reducing (H_2S/H_2 labeled as "-S") or oxidizing (Air/H_2S labeled as "-SO") conditions.

The concentration of H_2S was selected so as to exceed the 50–200 ppm sulfur concentration values typical of engine exhaust. For the first pre-treatment, ~150 mg of Pt/SBA-15 was heated to 250 °C in Ar and reduced in 100 mL min^{-1} of H_2 at 250 °C for 2 h. Then, a mixture containing 100 mL min^{-1} of 538 ppm H_2S/N_2 and 25 mL min^{-1} H_2 was flowed through the catalyst bed for 2 h, and the presence of sulfur in the effluent was verified by the formation of the precipitate silver sulfide while the effluent was bubbled through a solution of 1000 ppm $AgNO_3$ (Fluka Scientific, certified ACS). Weakly adsorbed sulfur was removed by reducing the catalyst in H_2 for 2 h at 250 °C before the samples were cooled in Ar and exposed to air. The second pre-treatment consisted of room-temperature exposure to flowing air (~100 mL min^{-1}) for about 20 min followed by a temperature ramp to 150 °C to calcine the sample for 30 min at 150 °C. The catalysts (~150 mg) were purged in Ar at 150 °C and treated in 538 ppm H_2S/N_2 for 2 h, all at a constant flow rate of 100 mL min^{-1}. The same $AgNO_3$ solution was used to verify the presence of sulfur flowing through the catalyst bed. After the (second) sulfidation treatment, the reactor was flushed with Ar for 15 min before increasing the temperature to 250 °C for reduction in 100 mL min^{-1} flow of H_2 for 1 h. Based on previous observations [51], the sample was heated in 100 mL min^{-1} Ar to 350 °C and treated in air for 5 h to decompose any bulk PtS into SO_2 and thus prevent undesirable contaminations in the NO oxidation kinetic reactor and instruments. During either sulfur pre-treatment, the 150 mg of Pt/SBA-15 catalyst containing about 10^{-6} moles of surface Pt was exposed to a total of 3×10^{-4} moles of H_2S.

The two sulfur treatments were intended to poison the catalysts to different degrees so as to explore possible correlations with the NO oxidation rate. Under reducing conditions, the S-free metallic catalysts samples were exposed to a mixture of H_2S/H_2 at 250 °C. The introduction of H_2 in the feed will shift the equilibrium toward H_2S, preventing the formation of large quantities of bulk platinum sulfide (which could lead to particle sintering) and also maintaining a gradientless poisoning process throughout the catalyst bed. At the poisoning conditions ($P_{H2S}/P_{H2} = 2 \times 10^{-3}$, 250 °C, 2 h), enough sulfur is available to reach saturation coverage, typically around 0.4–1.0 for Pt depending on temperature and sulfur concentration. The second sulfur pre-treatment aimed to poison Pt to a greater extent by oxidizing the surface and then reacting the platinum oxides with H_2S to form stable (at $T > 350$ °C) bulk PtS. In addition, hydrogen was not included in the feed, and the temperature during the sulfur treatment was lowered to 150 °C to favor the equilibrium toward adsorbed sulfur.

2.6. X-ray absorption spectroscopy (XAS) experiments

X-ray absorption measurements were taken at the Advanced Photon Source in Argonne National Laboratory using the insertion-device beam line of the Materials Research Collaborative Access Team (MRCAT). To minimize the background from harmonics, a cryogenically cooled double-crystal Si(1 1 1) monochromator and an uncoated glass mirror were used. During measurements, the monochromator was scanned constantly, and the data were integrated over 0.5 eV for 0.07 s per data point. All experiments were done in transmission mode. To optimize the current (10^9–10^{10} photons detected per second) with a linear response, a mixture of 10% Ar in N_2 (10% adsorption) was flown into the initial ionization chamber, and a mixture of 80% Ar in N_2 (70% adsorption) was used for purging the transmission ionization chamber. Energy calibration was done by simultaneously acquiring the spectrum of a platinum foil.

A cylindrical holder containing up to six catalyst pellets was used for the transmission XAS experiments. The thickness of the Pt/SBA-15 pellets (typically 40–70 mg of catalyst) was chosen to yield about 2.0 total absorbance (μx) at the Pt L_{III} edge and a Pt edge step ($\Delta\mu x$) of about 0.5. The measurements were taken on the clean and sulfided Pt/SBA-15 (2.3 nm, 3.8 nm, and 9.0 nm) catalysts. The XAS were collected after the following *ex situ* pre-treatments done on both clean and sulfided samples: (i) after reduction in 3.4% H_2/He at 300 °C for 1 h followed by purging with He for 10–20 min while cooling to room temperature and (ii) after exposure to the standard gas composition for NO oxidation (300 ppm NO, 170 ppm NO_2 and balance air) for 1 h at 300 °C and 350 mL min^{-1} followed by purging with He while cooling to room temperature (*Short* NO_x). For clean samples, a second pre-treatment was done consisting of exposing the samples to a highly oxidized NO_x gas mixture of 200 ppm NO, 500 ppm NO_2, and balance air for 18 h at 300 °C and 350 mL min^{-1} followed by purging with He while cooling (*Long* NO_x). The catalysts were analyzed in a continuous-flow EXAFS reactor cell (46 cm long, 1.9 cm diameter) fitted at both ends with polyimide windows and valves to isolate the reactor from the atmosphere. All the spectra were obtained at room temperature.

In situ XANES experiments were done on all the S-free Pt/SBA-15 catalysts using the same procedures described above. The analysis was performed on these catalysts for each of the following pre-treatments: (i) reduction in 2–4% H_2/He at 250 °C for 30 min or until the EXAFS showed no Pt–O backscatter followed by (ii) purging in He at 250 °C for about 5 min and (iii) exposure to NO oxidation reaction conditions, similar to those used for the kinetic measurements (300 ppm NO, 170 ppm NO_2, 10% O_2, balance He, 250 °C). The XAS spectra were collected at 90-s intervals starting at 210 s after introducing the gases. All the data were obtained at 250 °C until no significant changes were seen.

Reference compounds were used to correct for phase shifts and backscattering amplitudes and for fitting the XANES data. For Pt^0 (XANES) and the Pt–Pt bond distance (EXAFS), a Pt foil was used. Similarly, the reference for Pt^{2+} was taken from an oxidized (100 °C) 1 nm Pt/SiO_2, which showed 4 Pt-O bonds and no metallic Pt in the EXAFS. Phase and amplitude reference for Pt–S was obtained from H_2PtCl_6 with a Pt–Cl distance of 2.32 Å. Note that scattering is dependent on the number of electrons of the neighbor and is identical for scattering pairs that differ by only a few electrons. Thus, Pt–Cl is a good reference for the Pt–S coordination in these samples. Lastly, a XANES spectrum for Pt^{4+} was collected from transmission data on $Na_2Pt(OH)_6$ at 25 °C. The EXAFS data were processed and analyzed using WINXAS97 software [52]. A least-squares fit in *R*-space of the coordination k^2-weighted Fourier transform data allowed the calculation of the nearest neighbor first-shell Pt–O, Pt–S, and Pt–Pt parameters. The data with k^1 and k^3 weightings also resulted in satisfactory fits with negligible variation in the parameters.

2.7. X-ray photoelectron spectroscopy (XPS) measurements

A Kratos Ultra DLD SPS spectrometer was used for the analysis of sulfur species on the Pt/SBA-15 sample with 2.2 nm average Pt particle size. A pellet of about 1.42 cm in diameter and 1.3 mm thickness was prepared by pressing about 100 mg of the powdered catalyst in a bench-top hydraulic press under 5000 psi. Once loaded, the sample was treated with different gas mixtures and transferred to the UHV chamber without exposing it to the atmosphere. The analysis was performed on the sulfided Pt/SBA-15 (Pt/SBA-2.3-S) after: (i) short exposure to air at room temperature and (ii) reduction in 5%H_2/Ar at 300 °C for 1 h and then cooling in the same reducing mixture to 40 °C. Monochromatic Al Kα radiation was used to record the XPS spectra. All binding energy (BE) values were calibrated to the Si 2p energy of 104.3 eV with respect to the Fermi level [53]. The spectra were fitted using CasaXPS software (Casa Software Limited) assuming a line shape of a Hybrid

Doniach Sunjic/Lorentzian function [54] for Pt 4f and a pure Gaussian function for S 2s. The separation of the Pt 4f doublet was fixed to 3.3 eV, and the $4f_{5/2}$:$4f_{7/2}$ area ratio was set to 0.75. A Shirley-type background was fit and subtracted in the Pt 4f region [55].

3. Results

3.1. Effect of pre-adsorbed sulfur on NO oxidation kinetics

Kinetic measurements taken on the set of Pt/SBA-15 powder catalysts after *ex situ* treatments with H_2S along with the ones on the unsulfided samples are summarized in Table 1. The forward rate is reported as a turnover rate (TOR), which is defined as the number of moles of NO reacted per second per mole of surface Pt. The observed rates, r_{obs}, are corrected by a factor β, which is the approach to equilibrium using the expression:

$$r_f = r_{obs}(1-\beta)^{-1} \quad (1)$$

$$\beta = \frac{[NO_2]^2}{K[NO]^2[O_2]} \quad (2)$$

where K is the equilibrium constant of the overall reaction, $2NO_{(g)} + O_{2(g)} \rightarrow 2NO_{2(g)}$, as written. A typical range for β during our experiments was 0.01–0.15, verifying that the reaction was far from equilibrium. All values reported in Table 1 correspond to the ones measured after the catalysts were stabilized for 20–40 h, and no further deactivation was observed. Comparison of measured turnover rates with literature values is reported in Table 2.

A clear trend emerges from the data in Table 1 when one compares the TOR as a function of platinum particle size. There is an increase in the rate by about 60 times upon an increase in the average Pt particle size increased from 2 to 9 nm and by about 35 times for an increase in size from 2 to 4 nm. The results are in line with kinetic observations and DFT calculations for the effect of Pt particle size on the NO oxidation rate [37,38,56–60], which have suggested that smaller Pt particles exhibit lower rates because of their propensity to form inactive oxides. Alternatively, this dependency has also been explained in mechanistic terms from the difference in binding energy of chemisorbed oxygen on large Pt particles, which bind O^* more weakly than low coordinated Pt atoms typically present on smaller particles [43]. While the effect of pre-sulfiding the catalysts on the TOR was within a factor of 2, we observed that, as the Pt particle size increased, the variations in TOR with respect to the those on the S-free catalysts became more evident, yielding a higher rate for the samples treated in H_2S/H_2 and a lower rate for those treated in Air/H_2S. For the catalyst with the smallest Pt particle size (Pt/SBA-2.3), the TOR of the sulfided samples was nearly identical to the TOR of the clean catalyst. Similarly, the TOR for the catalysts with medium (Pt/SBA-3.8) and large (Pt/SBA-9.0) Pt particle size deviated by, at most, a factor of two. Such variations were not greatly influenced by the normalization to the Pt surface area since H_2S/H_2 treatments did not affect the Pt dispersion (as measured by CO titration) and only a slight sintering was observed after Air/H_2S treatments.

Table 2
Comparison with literature values for turnover rates of NO oxidation on Pt catalysts.

Catalyst	Pt loading (wt.%)	Pt dispersion (%)	TOR [a] (10^{-3} s^{-1})	Ref.
Pt/Al_2O_3	1.2	47	6.2	Weiss and Iglesia [43]
Pt/Al_2O_3	0.3	42	3.5	Mulla et al. [77]
Pt/SiO_2	2.5	14.2	42	Despres et al. [78]
Pt(1 1 1)			113[b]	Smeltz et al. [44]

[a] Turnover rate (TOR) at 300 °C corrected to 300 ppm NO, 170 ppm NO_2, 10%O_2, balance N_2. The active sites are the Pt atoms on the surface after reduction.
[b] Oxygen coverage of 0.76 ± 0.06 ML.

In the absence of sulfur, the kinetic parameters are in good agreement with our proposed mechanism [41] with a near-first-order dependence of the TOR on NO and O_2 and a near-negative-first-order dependence on NO_2 and an apparent activation energy (E_a) varying from 82 ± 2 to 102 ± 4 kJ mol^{-1}. As will be discussed in later sections, the values of E_a reported in Table 1 were obtained after the catalysts were stabilized for over 40 h on stream and they differ (by about 20–40 kJ mol^{-1}) from the E_a observed with shorter time on stream (TOS). Within experimental error, the addition of sulfur by H_2S/H_2 showed no effect on the apparent activation energy or the dependence on gas composition for any of the Pt/SBA-15 catalysts as the Pt particle size varied. A similar outcome was observed when the catalysts were oxidized prior to the second sulfur treatment at 150 °C. Given that the second sulfur treatment caused no differences in TOR, it is unlikely that the orders of reaction, which proved to be the less-sensitive parameters, were affected. To explore the possibility of sulfur desorbing/reacting during reaction, we also compared the transient measurement of the rate as shown in Fig. 1 for Pt/SBA-2.3 and correspondingly in Fig. S1 for Pt/SBA-3.8 and Fig. S2 for Pt/SBA-9.0 included in the Supplemental information section. The similarities in the shape of the transient-rate-versus-time curves suggest the existence of a source of deactivation that does not depend on the presence of sulfur and confirm that the NO oxidation reaction is insensitive to the presence of pre-adsorbed sulfur on Pt/SBA-15 catalysts.

3.2. EXAFS and XPS characterization of the S-treated catalysts

The main goal of the EXAFS measurements was to study the local environment of the Pt atoms in search for evidence of the presence of sulfur. Fig. 2 shows the k^2-weighted Fourier transform (FT) collected on the set of fresh and sulfided Pt/SBA-2.3 and Pt/SBA-3.8 catalysts. The FT of the spectra resulted in backscattering signal

Table 1
Summary of NO oxidation kinetics on Pt/SBA-15 samples as a function of particle size and different sulfur pre-treatments.

Catalyst	D (%) (d, nm) [a]	TOR [b] (10^{-3} s^{-1})	E_a (kJ mol^{-1})	NO order	O_2 order	NO_2 order
Pt/SBA-2.3	47 (2.3)	1.1 ± 0.1	82 ± 2	1.06	0.86	−0.95
Pt/SBA-3.8	29 (3.8)	38 ± 2	89 ± 7	1.04	0.86	−1.02
Pt/SBA-9.0	12 (9.0)	67 ± 6	102 ± 4	0.90	0.79	−1.00
Pt/SBA-2.3-S	49 (2.2)	1.2 ± 0.1	85 ± 5	0.93	1.07	−0.84
Pt/SBA-3.8-S	32 (3.4)	57 ± 2	82 ± 4	0.94	0.87	−1.22
Pt/SBA-9.0-S	11 (10.1)	136 ± 3	94 ± 3	1.17	0.86	−1.16
Pt/SBA-2.3-SO	41 (2.7)	1.4 ± 0.1	69 ± 7			
Pt/SBA-3.8-SO	25 (4.4)	26 ± 2	111 ± 8			
Pt/SBA-9.0-SO	10 (11.0)	49 ± 5	99 ± 8			

[a] Average Pt particle size from CO titration, calculated using d (nm) ≈ 1.1/(Pt dispersion, D).
[b] Turnover rate (TOR) at 300 °C measured at 300 ppm NO, 170 ppm NO_2, 10%O_2, balance N_2 after stabilization for >40 h, and normalized by the surface Pt atoms measured by CO titration.

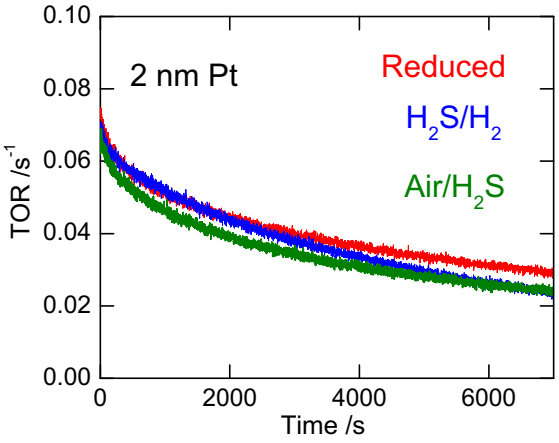

Fig. 1. Transient NO oxidation TOR measurements for the first 2 h on stream for 2.4% Pt/SBA-15 (Pt/SBA-2.3), Pt/SBA-2.3-S and Pt/SBA-2.3-SO at 300 °C and 300 ppm NO, 170 ppm NO_2, 10%O_2, balance N_2.

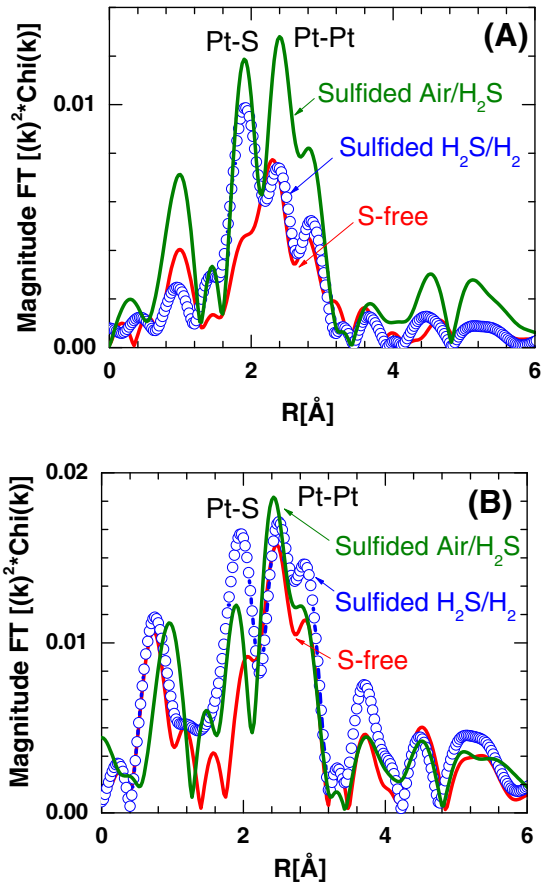

Fig. 2. Comparison of the magnitude of the Fourier transform EXAFS (k^2: Δk = 2.8–11 Å^{-1}, ΔR = 1.5–3.1 Å) for the set of clean and sulfided (A) 2.4% Pt/SBA-15 (Pt/SBA-2.3) and (B) 1%Pt/SBA-15 (Pt/SBA-3.8) catalysts. The data were collected after reduction at 300 °C in 3.4%H_2/He for 1 h and purging in He to room temperature.

corresponding to both Pt–Pt and Pt–S bonds, confirming the presence of sulfur on the reduced catalysts. Fitting of the EXAFS in Table S1 resulted in bond distances of 2.74 ± 0.02 Å for Pt–Pt and 2.28 Å for Pt–S. Table S1 also shows that Pt–S bonds were present on the reduced Pt/SBA-2.3-SO and Pt/SBA-3.8-SO catalysts. As the Pt particle size increases, the signal is dominated by the bulk structure and therefore, the relative intensity of the Pt–S signal decreases, making it more difficult to resolve it from the Pt–Pt backscattering contribution. As a consequence, it was not possible to detect Pt–S bonds on Pt/SBA-9.0-S (Fig. S3, Table S1).

To understand the state of sulfur under reaction conditions, EXAFS were collected after treating the samples *ex situ* in a typical NO oxidation mixture for 1 h (*Short* NO_x) and also after a subsequent reduction to study the reversibility of the Pt–S bonds. Fig. 3 shows the corresponding FT EXAFS for the case of the highly dispersed (Pt/SBA-2.3) catalyst. The results indicate that all the Pt–S backscattering vanished after NO oxidation, leaving only Pt–O contributions at a distance of 2.04 Å (Table S1). This is consistent with the XANES fittings that show that Pt is oxidized after exposure to NO_x. Interestingly, when the sample was reduced after NO oxidation, the intensity (in Fig. 3) and the coordination number (in Table S1) of the Pt–S bonds were completely recovered. This interaction was further confirmed by the presence of Pt–S backscattering on a reduced catalyst that was previously aged by exposure to reaction conditions for a long time on stream (>40 h). Similar Pt–Pt and Pt–S coordination numbers and bond distances were obtained on this aged catalyst as seen on the fresh one (Table S1). A qualitative comparison of the FT EXAFS on fresh and aged Pt/SBA-2.3-S catalysts is presented in Fig. S4.

The sulfided Pt/SBA-2.3-S sample was also analyzed by XPS in order to identify the chemical states of sulfur and estimate surface coverage. Fig. 4 shows the S 2s spectra obtained for Pt/SBA-2.3-S

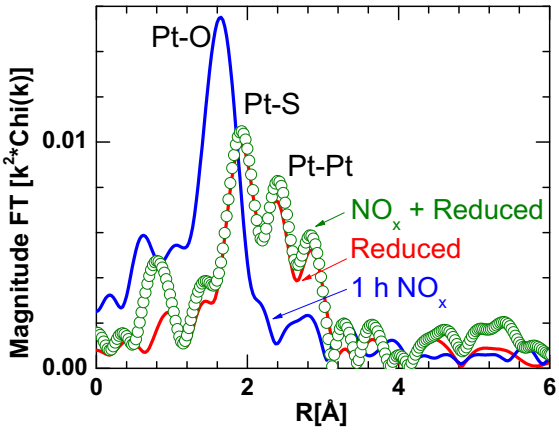

Fig. 3. Magnitude of the Fourier transform EXAFS (k^2: Δk = 2.8–11 Å^{-1}, ΔR = 1.5–3.1 Å) for the sulfided 2.4%Pt/SBA-15 (Pt/SBA-2.3-S) catalyst after a series of *ex situ* treatments. The NO_x treatment consisted of flowing a NO_x gas mixture of 300 ppm NO, 170 ppm NO_2 in air for 1 h at 300 °C, and 350 mL min^{-1} total flow rate.

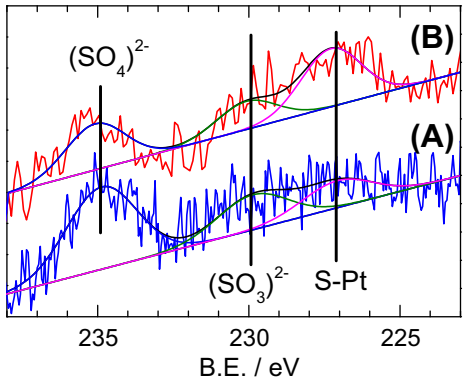

Fig. 4. XPS spectra in the S 2s region for the sulfided 2.4%Pt/SBA-15 (Pt/SBA-2.3-S) catalyst after (A) sulfur treatment and exposure to ambient conditions and (B) after reduction in 5%H_2/Ar for 1 h at 300 °C followed by cooling in the same reducing mixture to 40 °C.

catalyst after the two different conditions described in Section 2.7. The S 2s region was chosen for analysis since the main sulfur peaks in the 2p region were not observed due to overlapping by inelastic losses from the nearby Si 2s peak at 154.94 eV. Three types of sulfur species can be suggested from the XPS spectra, based on previous findings: (i) chemisorbed sulfur on platinum, S–Pt, located at 226–227 eV [61], (ii) adsorbed SO_3^{2-} species at 229–230 eV [61], and (iii) adsorbed SO_4^{2-} at 234–235 eV [62,63]. Quantification of relative atomic ratios, FWHM, and peak positions for sulfur species are summarized in Table 3 along with the corresponding values for Pt $4f_{7/2}$ and Pt^{2+} $4f_{7/2}$. The accuracy of the measurements is ±0.2 eV for the binding energy and ±0.4 eV for the FWHM. By comparing the atomic ratios of S-containing species after exposure to air and reduction at 300 °C, it is observed that the reduction treatment was able to increase the sulfide intensity by 21%. Such increase is accompanied by a decrease of 12% and 9% in S^{4+} and S^{6+} intensities, respectively. Here, the total sulfur intensity for both analysis conditions differed only by 3%.

Under the assumption that all sulfur species are adsorbed on Pt, a surface coverage (θ_s) of 0.7–0.9 ML was calculated by dividing the atomic ratios of sulfur and surface platinum (see Table S3). Since the particles on Pt/SBA-2.3-S are small, we assumed that the intensity of surface Pt is proportional to its total intensity multiplied by the dispersion. If only sulfide and sulfite species are assumed to interact with Pt, then θ_s = 0.4–0.5 ML, and if sulfides are the only adsorbed species, then θ_s was only about 0.2–0.3 ML. If one assumes that, after reduction at 300 °C, no Pt^{2+} comes from surface oxides but from Pt−S, a sulfur coverage around 0.65–0.7 ML can be estimated by dividing the atomic ratio of Pt^{2+} by that of total surface platinum (Pt^0 and Pt^{2+}). Also, the results from Table 3 confirmed that short exposures to ambient conditions after H_2S/H_2 only increased the surface oxidation by 10% compared with the reduced catalyst. The Pt $4f_{7/2}$ peak for the reduced sample was observed at 71.5–71.6 eV, which is in line with reported values for reduced platinum on Pt/SBA-15 [64].

3.3. Quantification of sulfur coverage by H_2 chemisorption–titration methods

Measurements of Pt surface area by chemisorption methods are summarized in Table 4. From the data, two trends emerged. First, the dispersion calculated from hydrogen chemisorption was significantly lower than those from CO or H_2 titration on all samples, with the exception of the one with the largest Pt particle size (Pt/SBA-9.0-S). However, the dispersion from titration of surface oxygen with hydrogen yielded values similar to those calculated from the CO titration method. Based on the EXAFS results, if one assumes that oxidation allows oxygen to occupy all the Pt sites regardless of the presence of sulfur and that the same (Pt:O) stoichiometry is preserved, then a surface coverage can be estimated by taking the ratio:

$$\theta_s = \frac{\frac{2}{3}(H_2|_{titration}) - 2(H_2|_{chem})}{\frac{2}{3}(H_2|_{titration})} \quad (3)$$

where the numbers in parenthesis are the specific gas uptake ($mL\,g^{-1}$) as measured by chemisorption and titration of hydrogen.

Table 4
Estimation of sulfur coverage on Pt/SBA-15 samples by chemisorption.

Catalyst	Pt dispersion (%)			θ_s
	CO titration	H_2 chem.	H_2 titration	
Pt/SBA-2.3	50 ± 5	49 ± 5	55 ± 2	
Pt/SBA-3.8	22 ± 3	22 ± 3	20 ± 1	
Pt/SBA-9.0	10 ± 1	8 ± 1	8 ± 1	
Pt/SBA-2.3-S	46 ± 4	18 ± 5	47 ± 4	0.6 ± 0.12
Pt/SBA-3.8-S	31 ± 2	9 ± 1	21 ± 3	0.5 ± 0.24
Pt/SBA-9.0-S	11 ± 1	9 ± 1	9 ± 1	0.0 ± 0.30
Pt/SBA-2.3-SO	52 ± 11	10 ± 1	47 ± 1	0.8 ± 0.02
Pt/SBA-3.8-SO	25 ± 1	8 ± 1	25 ± 1	0.7 ± 0.16
Pt/SBA-9.0-SO	7 ± 1	2 ± 1	8 ± 1	0.7 ± 0.42

The results for θ_s in Table 4 range from 0.5 to 0.8 and reveal that sulfidation under reducing conditions was not sufficient to poison the catalyst with the largest mean particle size (Pt/SBA-9.0-S). Interestingly, the second sulfur treatment, i.e., 538 ppm H_2S/N_2 over the pre-oxidized catalyst, effectively poisoned around 70% of the surface of reduced platinum on all samples regardless of particle size.

3.4. XAS evidence for deactivation during NO oxidation

Following previous studies on NO oxidation and NO_2 dissociation [36,38], which showed that deactivation is likely to be caused by platinum oxidation, we performed a series of *in situ* XANES experiments on the set of Pt/SBA-15 catalysts to investigate the chemical state of Pt under reaction conditions. After the catalysts were reduced and purged in He, they were exposed to the NO oxidation mixture, and the XANES spectra were collected every 60–120 s. Our results indicate that Pt oxidizes with increasing time on stream (TOS) in all the samples, but the fraction of Pt^0 strongly depends on the particle size, as shown in Fig. 5. The Pt^0 fraction seemed to reach a steady value after 10 min on stream in all cases. While Pt/SBA-2.3 shows complete oxidation of Pt, only 40% and 20% of the Pt gets oxidized on Pt/SBA-3.8 and Pt/SBA-9.0, respectively. That the greatest decay in metallic character occurred during the first 400 s does not explain the persistent decrease in turnover rate observed in Fig. 1 under similar conditions. Since the *in situ* experiments were done within 25 min and our steady state kinetic measurements required at least 16 h for stabilization, a second set of experiments was conducted to verify the state of Pt after longer time on stream (TOS).

The S-free Pt/SBA-15 catalysts were pre-treated *ex situ*, as described in Section 2.6, and the results are summarized in Table S2. A treatment in 4%H_2/He at 300 °C was sufficient to completely reduce platinum, according to the fitted XANES spectra. The Pt particle sizes were estimated from the coordination numbers using previous calibrations. These results are in good agreement with the corresponding values for dispersion obtained by the independent CO titration method reported in Table 1. The Pt–Pt bond distance on reduced catalysts was around 2.76 ± 0.02 Å, except for Pt/SBA-2.3, where a shorter distance of 2.66 ± 0.01 Å was observed. This contraction of the Pt bond distance occurs in the absence of chemisorbed species when the particles are small

Table 3
XPS S 2s and Pt $4f_{7/2}$ peak positions, FWHM and relative atomic ratios (R.A.) for the sulfided 2.4%Pt/SBA-15 catalyst (Pt/SBA-2.3-S).

Treatment	S–Pt, 2s			SO_3^{2-}, 2s		SO_4^{2-}, 2s		Pt, $4f_{7/2}$			Pt^{2+}, $4f_{7/2}$	
	BE (eV)	R.A. (%)	FWHM (eV)	BE (eV)	R.A. (%)	BE (eV)	R.A (%)	BE (eV)	R.A. (%)	FWHM (eV)	BE (eV)	R.A. (%)
As received [a]	227.1	0.089	2.9	229.9	0.085	234.9	0.158	71.5	0.58	2.2	72.9	0.22
5%H_2/He [b]	227.2	0.128	2.7	230.0	0.037	235.0	0.103	71.4	0.57	2.3	72.8	0.24

[a] After H_2S/H_2 treatment and exposure to ambient conditions.
[b] Reduction in 5%H_2/Ar at 300 °C for 1 h, then cool in reducing mixture to 40 °C.

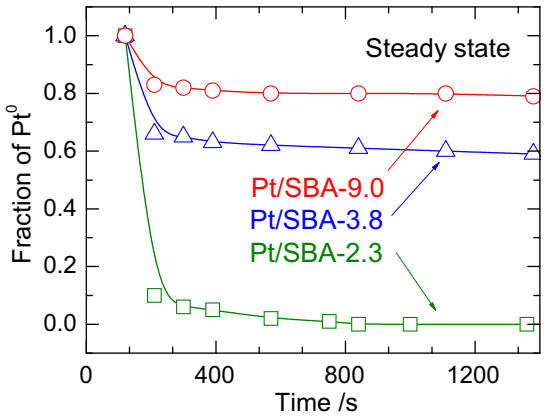

Fig. 5. Fraction of Pt^0 vs. time on stream measured by *in situ* XANES from 11.54 to 11.96 keV for all unsulfided Pt/SBA-15 catalysts. Time zero corresponds to the measurement in He at 250 °C immediately following the 250 °C reduction in 3.4% H_2/He and preceding the NO oxidation reaction (300 ppm NO, 170 ppm NO_2, 10% O_2, He at 250 °C).

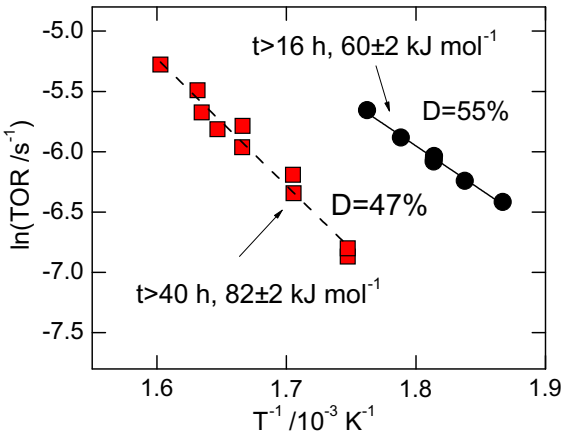

Fig. 6. Arrhenius plot for NO oxidation on 2.4%Pt/SBA-15 (Pt/SBA-2.3) showing changes in turnover rate (TOR) and E_a with time. TOR measured at 260–350 °C, 1 atm, and base case conditions. Platinum dispersion (D) was measured by CO titration.

(1–3 nm) [65]. This phenomenon is not unique to Pt as it has also been observed on catalysts with small Au particles [66]. The degree of Pt oxidation was measured after a short (1 h) exposure to NO oxidation conditions and resulted in values identical to those observed by *in situ* XANES experiments. The fitted XANES spectra suggest the formation of PtO on all three catalysts and PtO_2 on Pt/SBA-2.3 only. The XANES and EXAFS data are consistent with the oxidation of Pt as evidenced by the reduction in Pt–Pt coordination number (CN) and the associated increase in CN for Pt–O. Later, the samples were subjected to a long pre-treatment (*Long NO_x*) under oxidizing conditions. No changes in oxidation state were detected on the samples with medium and large average particle sizes, namely Pt/SBA-3.8 and Pt/SBA-9.0. However, a 20% increase in PtO_2 was seen on Pt/SBA-2.3. The particle size obtained from fitting the EXAFS also showed that the catalyst did not suffer from sintering during the time period of the experiments.

3.5. Instability of kinetic parameters with time on stream (TOS)

One of the reasons why we emphasized catalyst deactivation when measuring the NO oxidation kinetics was the change in parameters with TOS. An apparent steady state of the rate was maintained after the fresh catalysts were stabilized for 2–4 h, but as the exposure time increased, the catalysts showed further deactivation. As presented in Fig. 6 for Pt/SBA-2.3, the rate stabilized again after 40 h of exposure at lower levels with an apparent activation energy about 20 kJ mol^{-1} higher than previously measured. This aging phenomenon is not dependent on the type or geometry of the support since we also observed changes in E_a on a Pt/Al_2O_3 monolith catalyst (Fig. S5). In this case, our experiments indicated that after exposure to reaction conditions for 40 h or more, the (~30 kJ mol^{-1}) increase in E_a was maintained but the turnover rate continued to decrease with time on stream up to seven times (t > 150 h) compared with the rate measured after 40 h of reaction. As noted in Fig. S5, during the course of these experiments, we observed less than 10% decrease in metal dispersion, which indicated that no significant sintering occurred.

A summary of the observed changes in E_a on the Pt/SBA-15 catalysts is presented in Table 5. After a stabilization period of 16 h, the E_a on all samples was consistently around 60–68 kJ mol^{-1}. After deactivation for more than 40 h, E_a increased to about 90 ± 10 mol^{-1} on all the Pt/SBA-15 catalysts. The data in Table 5 are for catalysts that showed no further deactivation during the measurements of the activation energy.

Table 5
Summary of observed changes in turnover rate (TOR) and E_a for Pt/SBA-15 catalysts as a function of time on stream (TOS).

Catalyst	D (%) (d, nm) [a]	TOR [b] (10^{-3} s^{-1}) (E_a, kJ mol^{-1})	
		TOS > 16 h	TOS > 40 h
Pt/SBA-2.3	47 (2.3)	3.8 ± 0.5 (60 ± 2)	1.1 ± 0.1 (82 ± 2)
Pt/SBA-2.3-S	49 (2.2)	3.7 ± 0.3 (59 ± 3)	1.2 ± 0.1 (85 ± 5)
Pt/SBA-3.8	29 (3.8)	126 ± 6 (58 ± 3)	38 ± 2 (89 ± 7)
Pt/SBA-9.0	12 (9.0)	151 ± 1 (66 ± 2)	67 ± 6 (102 ± 4)

[a] Average Pt particle size by CO titration, calculated using d (nm) ≈ 1.1/(Pt dispersion, D).
[b] Turnover rate (TOR) measured at 300 °C, 1 atm and 300 ppm NO, 170 ppm NO_2, 10%O_2, balance N_2.

4. Discussion

4.1. Effect of sulfur on NO oxidation

After treatment of the samples in two different S-containing environments, the TORs after stabilization on Pt/SBA-15 catalysts were identical within a factor of two, as shown in Table 1. All TORs on Pt/SBA-15 compared within a factor of 5 (Table 2) to literature values on other Pt catalysts with similar dispersions. Regarding sulfur effects on the NO oxidation rate, previous studies [6,12,16,17] on Pt/Al_2O_3 have reported a beneficial result when adding SO_2 in the feed stream. The increase in NO_2 production was explained as being a consequence of S-promoted sintering and the resulting decrease in Pt oxide formation. This is not our case, as the CO titration and EXAFS coordination numbers (Table S1) suggest that no significant sintering had occurred on Pt after the *ex situ* sulfur treatments. Note that CO titration was not able to capture the expected decrease in surface area on any of the sulfur-poisoned catalysts. Nonetheless, the dispersion values estimated by this technique were used to normalize the rates because the catalyst operates under oxidation conditions. Other researchers have proposed that adsorbed sulfur in the form of sulfite or sulfate species can withdraw charge from neighboring Pt and thus influence to keep its reduced character [67]. For systems that suffer from deactivation due to Pt oxidation, the addition of sulfur may increase the stability of the catalyst at the cost of blocking a fraction of active sites, but we have seen no loss of surface Pt under oxidizing reaction conditions. Additionally, we measured no drastic changes in E_a and reaction orders with either of the two

sulfur treatments. The changes that were observed were similar to those for unsulfided samples, and we attribute them to catalyst instability rather than the presence of sulfur. These results indicate that sulfur is not playing an active role in the NO oxidation mechanism. Overall, the kinetic measurements suggest that under our experimental conditions, the reaction is insensitive to the presence of pre-adsorbed sulfur on all Pt/SBA-15 catalysts.

As pointed out in Figs. S1 and S2, the catalysts deactivated during reaction to different degrees depending on the average Pt particle size. For example, the turnover rate after stabilization (>40 h) was found to be about 50 times lower than the initial rate on the set of Pt/SBA-2.3 samples with the smallest particle size (2 nm). Correspondingly, the initial rate on the set of Pt/SBA-3.8 and Pt/SBA-9.0 catalysts decayed about 20 times after stabilization. When comparing the transient rates, we observed that catalyst deactivation is independent of the presence of pre-adsorbed sulfur. This suggests that sulfur adsorbed preferentially on kinetically irrelevant sites, namely sites that become inactive even in the absence of sulfur. The number of these sites is a function of the particle size distribution of each sample. Alternatively, sulfur may also adsorb on active sites but it is displaced by oxygen shortly after introducing the reactants such that the observed rates are effectively equal.

4.2. EXAFS/XPS/Chemisorption analysis for sulfur

The kinetic measurements showed no apparent effect of sulfur, but the EXAFS experiments clearly verified the presence of Pt–S bonds on the reduced catalysts. The FT of the EXAFS raw data presented in Fig. 2 shows that both sulfur treatments were able to partially sulfide Pt on Pt/SBA-2.3 and Pt/SBA-3.8. Even though Pt–S bonds could not be resolved on the sample with the highest average Pt particle size (Pt/SBA-9.0-S), one cannot rule out the possibility of sulfur adsorption without further verification. This ambiguity is caused by the increased magnitude of the characteristic Pt–Pt shoulder overlapping the EXAFS from the Pt–S bonds (Fig. S3). As presented in Table S1, the EXAFS fit confirmed the presence of Pt–S backscattering at a distance of 2.25–2.28 Å with a first-shell CN around 1 on the samples with 2 and 4 nm average Pt cluster size. The Pt–S distance we observed is shorter than the one for bulk PtS (2.31 Å) [22,29,68] or PtS_2 (2.40 Å), reflecting the fact that sulfur is chemisorbed on metallic platinum.

The results from EXAFS on the reduced Pt/SBA-2.3-S are in line with the XPS (Table S3) and chemisorption (Table 4) results that suggest sulfur coverages varying from 0.6 to 1 ML. Take as an example the absorption of sulfur on 3-fold hollow Pt sites on a closed packed surface (Scheme S1). Within the boundaries of a unit cell, there are four Pt atoms and four S atoms, giving a surface coverage equal or close to unity. In this lattice, each Pt has three sulfur neighbors, but only half of the Pt atoms in Pt/SBA-2.3-S are located on the surface (50% dispersion), which brings the averaged coordination number to 1.5, a value well within the experimental error of our XAS measurements.

Exposure to a mixture of NO_x at conditions similar to the ones used for our kinetic measurements revealed a reversible interaction between sulfur and platinum. After confirming the presence of Pt–S bonds on the catalysts after reduction, we observed that oxidation of NO_x resulted in first-shell backscattering from the Pt–O neighbors only. Interestingly, further reduction of the sample brought back the Pt–S bond contribution and the metallic character of the Pt, as can be seen in Fig. 3 and Table S1. Consistent with our kinetic measurements, two feasible interpretations of these results are (i) the formation of Pt–O–S–O_x species under oxidation conditions, as suggested by Gracia et al. [22], and (ii) sulfur displacement from surface Pt by oxygen and subsequent migration to the metal–support interface or even to regions on the support near Pt. This second hypothesis is supported by the chemisorption results in the sense that CO and H_2 titration methods, which titrate the adsorbed oxygen, were unable to differentiate the fraction of unpoisoned Pt, while H_2 chemisorption did. Both of these hypotheses are in line with the idea that sulfur remained near the Pt and was not removed from the catalysts. In fact, the EXAFS data for the reduced Pt/SBA-2.3-S verified the presence of sulfur after the catalyst was subjected to long exposures to NO_x mixtures during kinetic measurements (Fig. S4, Table S1). This finding is relevant as it reveals that sulfur was not fully removed from the vicinity of Pt under oxidation conditions, yet no detrimental effect on the rate was found.

Other researchers have observed a similar reversible behavior of sulfur on Ni-supported catalysts when attempting to regenerate them with oxygen. For example, Colby [69] reported that atmospheric pressure O_2 at 300 °C resulted in the rapid formation of a layer of nickel oxide. A reduction treatment with H_2 at 400 °C for 2 h reduced the metal and restored the sulfur layer on the surface. The use of surface-sensitive Auger spectroscopy allowed the authors to conclude that in the presence of high pressures (10–760 Torr) of oxygen, the formation of oxides (in 27–527 °C range) occurs faster than the rate of sulfur oxidation, and therefore, the poison is trapped underneath a layer of oxide. This picture, however, is not consistent with our EXAFS results because this technique provides a volume average of the type and number of neighboring atoms. If sulfur were to be buried below the surface, the Pt–S contribution should still be present along with Pt–O bonds, which is clearly not the case. Instead, the formation of Pt–O–SO_x species and/or the displacement of sulfur by oxygen to perimeter or support sites are more reasonable explanations for our results.

The XPS experiments on Pt/SBA-2.3-S gave further information on the chemical state of sulfur as the catalyst was exposed to different environments. The Pt/SBA-2.3-S catalyst was chosen for analysis since it had a higher Pt loading and dispersion, thus increasing the chances of observing surface sulfur. Despite the low concentration of sulfur, estimated from EXAFS to be about 0.06 wt.% on Pt/SBA-2.3-S, the S 2s XPS spectra shown in Fig. 4 allowed the identification of three chemical states of sulfur. Based on reported literature values for $ZnSO_4$ [62] and $PbSO_4$ [70], we suggest that the peak located at 235 eV corresponds to sulfate species. Similarly, we used the BE for $PbSO_3$ at 229.2 eV [71] and the corresponding one for S–Pt at 226.5 eV [61] to justify the presence of sulfite and sulfide species. When the sample was reduced in 5%H_2/Ar, the intensities of sulfite and sulfate species decreased, resulting in an equivalent rise of intensity for reduced sulfur, as shown in Table 3. These changes in sulfur oxidation state support the idea of sulfur being in the region of influence of Pt; however, the presence of S^{6+} after reduction opens the possibility of sulfur adsorption on the SBA-15 support. Since the precision of the data was insufficient to determine the fraction of sulfur species adsorbed on Pt, we estimated bounds on the surface coverages according to the measured XPS atomic ratios and which species were assumed to adsorb on the metal.

The results presented in Table S3 indicate that sulfur species could be covering the platinum surface in a range of 20–90%. Note than even if all sulfur species are assumed to adsorb on Pt, θ_s did not exceed 1, suggesting that under oxidation environments like those in the NO oxidation reaction, sulfur may be bonded to Pt as sulfites/sulfates. Although we do not have XPS evidence to distinguish the chemical state of sulfur during NO oxidation, previous studies on a model Pt(3 5 5) surface showed that sulfur transforms into the SO_4 intermediate during oxidation (6×10^{-7} mbar O_2 pressure) at 77 °C [72]. Therefore, is it feasible to propose that the formation of sulfates under NO oxidation conditions (10%O_2, 300 °C) must be favored. This picture of sulfates adsorbed on Pt is also consistent with the EXAFS data that suggest Pt–O–SO_x

formation on Pt/SBA-2.3-S and Pt/SBA-3.8-S after reaction. Based on the XPS evidence, however, we cannot exclude the possibility that sulfur species co-exist on support sites in light that formation of sulfates on other supports such as Al_2O_3 [21–23] or ZrO_2 [73] has been observed. For instance, it is possible that oxidation of sulfur to SO_x takes place on Pt followed by a partial migration of these species to interfacial or support sites.

Independent chemisorption measurements presented in Table 4 also support the hypothesis of sulfur displacement. The first indication comes from the similarities in available surface area between clean and sulfided catalysts when adsorbed oxygen was titrated by flowing CO. Second, the fact that similar dispersion values were obtained by using H_2 titration corroborates the finding that one oxygen atom per Pt site is available for reaction, regardless of the presence of sulfur. For this to happen, most of the sulfur would have to be displaced from Pt resulting in a layer of Pt–O. Another possibility can also be envisioned in which sulfur forms reactive Pt–O–SO_x species that interact with NO and NO_2 and effectively assume the same role as Pt alone in providing oxygen. If sulfur species were taking an active role in the reaction, however, one would expect to see changes in reaction orders and/or activation energies, which in our case were minimal. Furthermore, surface crowding by SO_x species might also be expected to affect the kinetics.

After reduction, the surface area measured by H_2 chemisorption decreased on all the samples but Pt/SBA-9.0-S, thus confirming that the titration results are not just a consequence of Pt being resistant to sulfidation under our experimental conditions. Based on these results, sulfur coverages were obtained by assuming that titration of surface oxygen measures the total available Pt area, while H_2 chemisorption only counts the unpoisoned Pt sites. According to the values of θ_s in Table 4, the samples with 2- and 4-nm Pt particles were poisoned to ~½ ML sulfur coverage under reducing conditions. Not surprisingly, the sample with large Pt clusters (9 nm) showed more resistance to sulfur as the noble character of Pt is enhanced with particle size. In fact, studies of single crystals [74] have shown that the heat of sulfur adsorption on Pt increases with surface roughness, which is an indicative of a selective poisoning process. Interestingly, the second sulfur treatment seemed more effective in poisoning most of the Pt surface (~0.7 ML) at all particle sizes. If our above assumptions are correct, the chemisorption results allowed not only an independent verification of the presence of sulfur but also a quantitative analysis on all of the Pt/SBA-15 samples.

In light of the strong evidence that sulfur interacts with Pt, reconciling the kinetic and spectroscopic data requires that the insensitivity of the NO oxidation to sulfur is caused by the greater affinity of Pt to form oxides versus sulfides. According to our XPS and chemisorption results, sulfur was able to at least partly cover the surface of Pt, and yet, when that sample was exposed to NO oxidation conditions, the transient and stabilized TORs did not correlate with the expected loss in active sites. In addition, the EXAFS data on S-treated samples after *Short NO_x* (Table S1) not only showed complete removal of Pt–S bonds but also indicated that Pt oxidized to the same extent as for the unsulfided catalysts (Table S2). If all the sulfur present after reduction formed Pt–O–SO_x species under NO_x mixtures, then at least the initial rate should have changed correspondingly. Therefore, migration of sulfur must occur to some extent, particularly on Pt sites that are likely to maintain their metallic character (and their activity) under NO oxidation conditions. On the other hand, sulfur may remain adsorbed on platinum sites in the form of sulfates, with increasing coverage as the Pt particles become smaller. Small Pt clusters are characterized by defect sites (step/kinks/terraces) that tend to form oxides and become inactive (or much less active), and their contribution to the observed rate is negligible, regardless of the presence of sulfur. Although the data do not provide sufficient information on how sulfur behaves during NO oxidation, they revealed that treating Pt with sulfur on a poor S-adsorbing support does not change the rate or the deactivation behavior caused by oxygen. These results on the effect of sulfur pointed out the importance of platinum oxidation on the short- and long-term stability of Pt for NO oxidation, as discussed in the next section.

4.3. Deactivation and instability of kinetic parameters

To address the question of deactivation caused by platinum oxidation, we performed a series of *in situ* XANES experiments as described in Section 2.6. The results shown in Fig. 5 clearly indicate that Pt oxidation occurred within the first 6 min on stream. However, the subsequent stabilization of the average oxidation state of Pt did not correlate with the continuous decay in activity observed in our kinetic measurements within a similar time period of 1500 s (Fig. 1). Differences in the results from the two experiments may arise from the fact that the XAS experiments were conducted on a cylindrical holder with the samples pressed into pellets. The space between the holder and the glass tube was not blocked, allowing most of the incoming gas flow to bypass the catalyst. As the gases diffuse inside the catalyst, the NO_2 concentration will increase to close to equilibrium levels, resulting in a high driving force for Pt oxidation. On the contrary, during our kinetic measurements, the gas is forced to pass through the catalyst bed, and the NO_x concentrations do not change significantly as we operate under differential conditions. In spite of the differences in the time scale for deactivation, the data in Fig. 5 show that under typical NO oxidation environments platinum oxides are readily formed especially as the particle size decreases.

Given that our kinetic data required long stabilization periods to measure reproducible values, we investigated the effect of prolonged time on stream (TOS) on the state of Pt by XANES. The results presented in Table S2 show that the degree of Pt oxidation after a 1-h *ex situ* NO_x treatment is identical to that achieved at steady state during the *in situ* XANES experiments (Table S4, Fig. 5). That the Pt oxidation state is invariant after 18-h exposure to a NO_2-rich gas mixture strongly suggests that no bulk oxidation takes place after long TOS. Only the catalyst with average 2-nm Pt particle showed an increase in oxidation with TOS, which is indicative of its greater instability. As the surface sensitivity of XANES decreases with increasing particle size, it is possible that the degree of surface oxidation on the 4- and 9-nm Pt clusters also increases with TOS, but XANES was unable to measure such changes. What is evident is that deactivation is not related to the formation of bulk oxides, but rather to a surface phenomenon, possibly caused by the slow oxidation of the surfaces of the relatively larger particles since we believe that platinum oxides are inactive compared to metal sites. In fact, recent DFT calculations [75] predict that NO oxidation on a PtO_2(1 1 0) surface will exhibit a TOR ($T = 600$ K, $P_{O2} = 0.1$, $P_{NO} = 3 \times 10^{-4}$, $P_{NO2} = 1.7 \times 10^{-4}$) of 5.1×10^{-13} s^{-1}, which is negligible relative to their calculated TOR of 1.9×10^{-4} s^{-1} on a Pt(1 1 1) with low oxygen coverage (3×10^{-6} ML). The discrepancy of two orders of magnitude in their calculated TOR with experimental work in our group [44] arises from the fact that only platinum sites with enough O coverage (0.4–0.8 ML) are responsible for the observed turnover rate. However, at these O coverages, Pt is metastable to the formation of inactive surface oxides, which results in catalyst deactivation.

The special emphasis we make on catalyst deactivation is justified by the observed changes in kinetic parameters with time on stream. During the course of the kinetic experiments, we have observed changes in TOR and E_a on both Pt/SBA-15 and Pt/Al_2O_3 catalysts (Fig. 6 and Fig. S5). As presented in Table 5, a 20- to 40-kJ mol^{-1} increase in E_a was measured for the Pt/SBA-15 catalysts

after aging for about 40 h on stream. We note that E_a values around 60 kJ mol^{-1} are representative of all catalysts after 16 h on stream and that after 40 h, greater increments in activation energies were measured with increasing Pt particle size. Since our XANES data indicated that no oxidation of bulk Pt occurs at extended times on stream, we believe that catalyst aging is driven by surface rearrangement and oxidation that only takes place over long exposure times. Further oxidation of the surface by a fraction of a monolayer would not be detectable by XANES. Such restructuring may change the resistivity of particles to oxidation by creating coordinately unsaturated sites that nucleate oxidation. As the number of such sites increases, the effect of aging with time on stream becomes more evident. We envision that small particles are likely to remain oxidized as reaction conditions changes, while a fraction of larger particles may oxidize on the surface, depending on the temperature and gas compositions. This behavior is supported by thermodynamic calculations, which suggest that under our typical operation conditions, Pt is in a metastable state between Pt with reactive chemisorbed oxygen and PtO_x [76]. Consequently, the changes we observe with time may just be a consequence of the continuous changes in platinum as it adjusts to varying conditions and relaxes toward the thermodynamically favored oxide state.

5. Conclusions

The kinetic and spectroscopic evidence presented here shows that the presence of pre-adsorbed sulfur on Pt/SBA-15 catalysts has no significant effect on the rate or the kinetics of the NO oxidation reaction. The insensitivity of the steady turnover rates to the presence of sulfur can be explained as a combination of two effects: (i) displacement of sulfur from Pt to interfacial or support sites driven by Pt oxidation and (ii) selective poisoning by S on coordinately unsaturated surfaces that are effectively inactive for NO oxidation, even in the absence of sulfur. This argument is based on EXAFS data that showed a complete reversal of Pt–S (observed after reduction) to Pt–O bonds when the catalysts are exposed to typical NO oxidation conditions. Both XPS and chemisorption measurements confirmed a substantial presence of sulfur on reduced Pt, reaching up to 0.8 ML coverage. Nevertheless, sulfur treatments failed to affect the catalyst performance under reaction conditions, leaving Pt oxidation as the main source of catalyst deactivation. This knowledge can be directly applied for designing better NSR formulations focusing on improving the selectivity of the support toward NO_x uptake (vs. SO_x) and the resistivity of Pt to form oxides. In that regard, our *in situ* XAS data on S-free Pt/SBA-15 and Pt/Al_2O_3 confirmed that the propensity to form oxides decreases with increasing particle size and revealed that on relatively large Pt clusters no bulk oxidation occurs with prolonged exposures to NO_x. Although the results showed an increase in Pt^{4+} on small particles (2 nm) after long times on stream, we conclude that those particles become inactive quickly by forming PtO. These findings are consistent with our theory that the active sites for NO oxidation are Pt surfaces that resist oxidation, while defect sites (omnipresent on the surface of small particles) quickly deactivate and do not turn over. Finally, we postulate that the long-term rate changes are caused by the rearrangement of Pt surfaces on medium (4–6 nm) and large particles (9–12 nm) possibly by additional oxidation by a fraction of a monolayer that leads to the formation of metastable surface oxides not detectable by XANES.

Acknowledgments

Support from the Department of Energy, Office of Basic Energy Sciences, Chemical Sciences, under Grant DE-FG02-03ER15408, is gratefully acknowledged. Use of the Advanced Photon Source was supported by the US Department of Energy, Office of Science, Office of Basic Energy Sciences, under Contract No. DE-AC02-06CH11357. We are greatly thankful to Dr. Dmitry Zemlyanov for collecting the XPS data and providing valuable comments on the data analysis and Professor R.M. Rioux for providing the Pt/SBA-15 samples.

Appendix A. Supplementary material

Supplementary data associated with this article can be found, in the online version, at doi:10.1016/j.jcat.2011.05.007.

References

[1] S. Roy, A. Baiker, Chem. Rev. 109 (2009) 4054–4091.
[2] A. Amberntsson, B. Westerberg, P. Engström, E. Fridell, M. Skoglundh, B.D.a.G.F. Froment, Stud. Surf. Sci. Catal. 126 (1999) 317–324.
[3] P. Engström, A. Amberntsson, M. Skoglundh, E. Fridell, G. Smedler, Appl. Catal. B 22 (1999) L241–L248.
[4] S.i. Matsumoto, Y. Ikeda, H. Suzuki, M. Ogai, N. Miyoshi, Appl. Catal. B 25 (2000) 115–124.
[5] A. Amberntsson, M. Skoglundh, M. Jonsson, E. Fridell, Catal. Today 73 (2002) 279–286.
[6] A. Amberntsson, M. Skoglundh, S. Ljungström, E. Fridell, J. Catal. 217 (2003) 253–263.
[7] J. Dawody, M. Skoglundh, L. Olsson, E. Fridell, J. Catal. 234 (2005) 206–218.
[8] E. Fridell, H. Persson, L. Olsson, B. Westerberg, A. Amberntsson, M. Skoglundh, Top. Catal. 16 (2001) 133–137.
[9] S. Elbouazzaoui, E.C. Corbos, X. Courtois, P. Marecot, D. Duprez, Appl. Catal. B 61 (2005) 236–243.
[10] D.H. Kim, Y.H. Chin, G.G. Muntean, A. Yezeretz, N.W. Currier, W.S. Epling, H.Y. Chen, H. Hess, C.H.F. Peden, Ind. Eng. Chem. Res. 45 (2006) 8815–8821.
[11] S. Poulston, R.R. Rajaram, Catal. Today 81 (2003) 603–610.
[12] A. Amberntsson, E. Fridell, M. Skoglundh, Appl. Catal. B 46 (2003) 429–439.
[13] J. Dawody, M. Skoglundh, E. Fridell, J. Mol. Catal. A: Chem. 209 (2004) 215–225.
[14] Y.Y. Ji, T.J. Toops, U.M. Graham, G. Jacobs, M. Crocker, Catal. Lett. 110 (2006) 29–37.
[15] O. Krocher, M. Widmer, M. Elsener, D. Rothe, Ind. Eng. Chem. Res. 48 (2009) 9847–9857.
[16] L. Olsson, H. Karlsson, Catal. Today 147 (2009) S290–S294.
[17] A. Toubeli, E.A. Efthimiadis, I.A. Vasalos, Catal. Lett. 69 (2000) 157–164.
[18] E.A. Efthimiadis, S.C. Christoforou, A.A. Nikolopoulos, I.A. Vasalos, Appl. Catal. B 22 (1999) 91–106.
[19] A.A. Nikolopoulos, E.S. Stergioula, E.A. Efthimiadis, I.A. Vasalos, Catal. Today 54 (1999) 439–450.
[20] C.C. Chang, J. Catal. 53 (1978) 374–385.
[21] P.D. Clark, N.I. Dowling, M. Huang, O. Okemona, G.D. Butlin, R. Hou, W.S. Kijlstra, Appl. Catal. A 235 (2002) 61–69.
[22] F.J. Gracia, S. Guerrero, E.E. Wolf, J.T. Miller, A.J. Kropf, J. Catal. 233 (2005) 372–387.
[23] J.C. Summers, Environ. Sci. Technol. 13 (1979) 321–325.
[24] H. Abdulhamid, E. Fridell, J. Dawody, M. Skoglundh, J. Catal. 241 (2006) 200–210.
[25] C.H. Bartholomew, G.D. Weatherbee, G.A. Jarvi, J. Catal. 60 (1979) 257–269.
[26] T. Wang, A. Vazquez, A. Kato, L.D. Schmidt, J. Catal. 78 (1982) 306–318.
[27] Y. Berthier, M. Perderea, J. Oudar, Surf. Sci. 36 (1973) 225–241.
[28] W. Heegemann, K.H. Meister, E. Bechtold, K. Hayek, Surf. Sci. 49 (1975) 161–180.
[29] J.R. Chang, S.L. Chang, T.B. Lin, J. Catal. 169 (1997) 338–346.
[30] P.J.F. Harris, Nature 323 (1986) 792–794.
[31] L.D. Schmidt, D. Luss, J. Catal. 22 (1971) 269–279.
[32] G.A. Somorjai, J. Catal. 27 (1972) 453–456.
[33] C.R. Apesteguia, C.E. Brema, T.F. Garetto, A. Borgna, J.M. Parera, J. Catal. 89 (1984) 52–59.
[34] M.V. Mathieu, M. Primet, Appl. Catal. 9 (1984) 361–370.
[35] A. Melchor, E. Garbowski, M.V. Mathieu, M. Primet, React. Kinet. Catal. Lett. 29 (1985) 371–377.
[36] J. Després, M. Elsener, M. Koebel, O. Kröcher, B. Schnyder, A. Wokaun, Appl. Catal. B 50 (2004) 73–82.
[37] S.S. Mulla, N. Chen, L. Cumaranatunge, G.E. Blau, D.Y. Zemlyanov, W.N. Delgass, W.S. Epling, F.H. Ribeiro, J. Catal. 241 (2006) 389–399.
[38] L. Olsson, E. Fridell, J. Catal. 210 (2002) 340–353.
[39] J. Segner, W. Vielhaber, G. Ertl, Isr. J. Chem. 22 (1982) 375–379.
[40] D.H. Parker, B.E. Koel, J. Vac. Sci. Technol. A 8 (1990) 2585–2590.
[41] S.S. Mulla, N. Chen, W.N. Delgass, W.S. Epling, F.H. Ribeiro, Catal. Lett. 100 (2005) 267–270.
[42] D. Bhatia, R.W. McCabe, M.P. Harold, V. Balakotaiah, J. Catal. 266 (2009) 106–119.
[43] B.M. Weiss, E. Iglesia, J. Phys. Chem. C 113 (2009) 13331–13340.
[44] A.D. Smeltz, R.B. Getman, W.F. Schneider, F.H. Ribeiro, Catal. Today 136 (2008) 84–92.
[45] R.M. Rioux, H. Song, J.D. Hoefelmeyer, P. Yang, G.A. Somorjai, J. Phys. Chem. B 109 (2005) 2192–2202.

[46] J.E. Benson, M. Boudart, J. Catal. 4 (1965) 704–710.
[47] R.J. Madon, M. Boudart, Ind. Eng. Chem., Fundam. 21 (1982) 438–447.
[48] F.H.M. Dekker, A. Bliek, F. Kapteijn, J.A. Moulijn, Chem. Eng. Sci. 50 (1995) 3573–3580.
[49] R.E. Hayes, S.T. Kolaczkowski, Catal. Today 47 (1999) 295–303.
[50] D.R. Lide (Ed.), CRC Handbook of Chemistry and Physics, 91st ed., CRC Press, Boca Raton, FL, 2011.
[51] B.L.K. Yang, H. Harold, Ind. Eng. Chem. Res. 33 (1994) 1090–1097.
[52] T. Ressler, J. Synchrotron Radiat. 5 (1998) 118–122.
[53] C.D. Wagner, W.M. Riggs, L.E. Davis, J.F. Moulder, G.E. Muilenberg, Handbook of X-ray Photoelectron Spectroscopy, 1st ed.., Perkin-Elmer Corporation, Eden Prairie, MN, 1979.
[54] S. Doniach, M. Sunjic, J. Phys. C: Solid State Phys. 3 (1970) 285–291.
[55] D.A. Shirley, Phys. Rev. B 5 (1972) 4709.
[56] S. Benard, L. Retailleau, F. Gaillard, P. Vernoux, A. Giroir-Fendler, Appl. Catal. B 55 (2005) 11–21.
[57] J.H. Lee, H.H. Kung, Catal. Lett. 51 (1998) 1–4.
[58] P.J. Schmitz, R.J. Kudla, A.R. Drews, A.E. Chen, C.K. Lowe-Ma, R.W. McCabe, W.F. Schneider, C.T. Goralski, Appl. Catal. B 67 (2006) 246–256.
[59] Y. Xu, R.B. Getman, W.A. Shelton, W.F. Schneider, Phys. Chem. Chem. Phys. 10 (2008) 6009–6018.
[60] E. Xue, K. Seshan, J.R.H. Ross, Appl. Catal. B 11 (1996) 65–79.
[61] M. Salmeron, R.J. Koestner, E.B. Kollin, J.L. Gland, Surf. Sci. 172 (1986) 668–690.
[62] B.R. Strohmeier, D.M. Hercules, J. Catal. 86 (1984) 266–279.
[63] B.R. Strohmeier, D.E. Levden, R.S. Field, D.M. Hercules, J. Catal. 94 (1985) 514–530.
[64] A.B. Chen, W.P. Zhang, X.Y. Li, D.L. Tan, X.W. Han, X.H. Bao, Catal. Lett. 119 (2007) 159–164.
[65] N. Guo, B.R. Fingland, W.D. Williams, V.F. Kispersky, J. Jelic, W.N. Delgass, F.H. Ribeiro, R.J. Meyer, J.T. Miller, Phys. Chem. Chem. Phys. 12 (2010) 5678–5693.
[66] J.T. Miller, A.J. Kropf, Y. Zha, J.R. Regalbuto, L. Delannoy, C. Louis, E. Bus, J.A. van Bokhoven, J. Catal. 240 (2006) 222–234.
[67] A.F. Lee, K. Wilson, R.M. Lambert, C.P. Hubbard, R.G. Hurley, R.W. McCabe, H.S. Gandhi, J. Catal. 184 (1999) 491–498.
[68] J.R. Chang, S.L. Chang, J. Catal. 176 (1998) 42–51.
[69] S.A. Colby, Auger study of oxidative removal of sulfur from nickel, in: University of Delaware, Newark, 1977.
[70] D.S. Zingg, D.M. Hercules, J. Phys. Chem. 82 (1978) 1992–1995.
[71] J.M. Thomas, R.H. Williams, M. Barber, I. Adams, J. Chem. Soc. Faraday Trans. 2 (68) (1972) 755.
[72] R. Streber, C. Papp, M.P.A. Lorenz, A. Bayer, R. Denecke, H.P. Steinruck, Angew. Chem., Int. Ed. 48 (2009) 9743–9746.
[73] M.-D. Appay, J.-M. Manoli, C. Potvin, M. Muhler, U. Wild, O. Pozdnyakova, Z. Paál, J. Catal. 222 (2004) 419–428.
[74] J. Benard, J. Oudar, N. Barbouth, E. Margot, Y. Berthier, Surf. Sci. 88 (1979) L35–L41.
[75] H.-F. Wang, Y.-L. Guo, G. Lu, P. Hu, J. Phys. Chem. C 113 (2009) 18746–18752.
[76] R.B. Getman, Y. Xu, W.F. Schneider, J. Phys. Chem. C 112 (2008) 9559–9572.
[77] S.S. Mulla, N. Chen, L. Cumaranatunge, W.N. Delgass, W.S. Epling, F.H. Ribeiro, Catal. Today 114 (2006) 57–63.
[78] J. Despres, M. Elsener, M. Koebel, O. Krocher, B. Schnyder, A. Wokaun, Appl. Catal. B 50 (2004) 73–82.